Sensing and Imaging (2021) 22:36
https://doi.org/10.1007/s11220-021-00359-x

ORIGINAL PAPER

Temperature and Relative Humidity Dependence of Quality Factors of MEMS Cantilever Resonators in Atmospheric Pressure

Quoc Cuong Le[1] · Minh Truong Phan[2] · Xuan Thang Trinh[3] · Huu Ly Truong[3] · Vo Ke Thanh Ngo[3] · Chi Cuong Nguyen[2,3]

Received: 4 March 2021 / Revised: 11 July 2021 / Accepted: 3 August 2021

Abstract
In this study, the effects of temperature (T) and relative humidity (RH) of moist air are discussed on the quality factors (Q-factor) of micro-electro-mechanical-system (MEMS) cantilever resonators in atmospheric pressure ($p = 101{,}325$ Pa). The dominant squeeze film damping (SFD) of MEMS cantilever resonators is studied by solving the modified molecular gas lubrication (MMGL) equation. Dynamic viscosity and Poiseuille flow rate of moist air are utilized to modify the MMGL equation as functions of temperature and relative humidity for wide range of accommodation coefficients (ACs). In atmospheric pressure, dynamic viscosity changes more significantly with temperature and relative humidity than that of Poiseuille flow rate. The dominant thermoelastic damping (TED) and support loss are also included to obtain the Q-factor in wide range of cantilever sizes (length, width, and thickness). Thus, dependence of Q-factors of MEMS cantilever resonators on temperature and relative humidity is discussed for wide range of ACs and cantilever sizes in atmospheric pressure. The results show that Q-factor could be increase at higher temperature and relative humidity or lower ACs. Dependence of Q-factor on temperature and relative humidity enhances considerably in greater length, greater width, and smaller thickness of cantilever. Maximum Q-factors with temperature and relative humidity can be obtained for wide range of ACs and cantilever sizes in atmospheric pressure.

Keywords Quality factor · MEMS cantilever resonators · Environmental effect · Temperature · Relative humidity · Atmospheric pressure

Nomenclature

ACs	Accommodation coefficients

✉ Chi Cuong Nguyen
cuong.nguyenchi@shtplabs.org

Extended author information available on the last page of the article

Published online: 11 August 2021

AFM	Atomic force microscope
d	Diameter of cross section of gas molecule
D	Inverse Knudsen number
D_p	Cantilever flexural rigidity
E	Young's modulus
f	Enhancement factor
FEM	Finite element method
h_0	Gas film spacing
i	Complex number
K_n	Knudsen number
L_b	Cantilever length
MEMS	Micro-electro-mechanical-systems
MMGL	Modified molecular gas lubrication
n_a	Number of moles of dry air
n_v	Number of moles of water vapor
N_a	Avogadro's number
p	Total atmospheric pressure
p_0	Reference pressure of gas
p_{sv}	Saturation pressure of water vapor
p_v	Partial pressure of water vapor
Q-factor	Quality factor
Q_P	Poiseuille flow rate
$\tilde{Q}_P$	Poiseuille flow rate for gas rarefied flow
Q_{sup}	Quality factor of support loss
Q_{SFD}	Quality factor of SFD
Q_{total}	Total quality factor
Q_{TED}	Quality factor of TED
R	Gas constant
RH	Relative humidity
sup	Support loss
SFD	Squeeze film damping
t	Time
T	Temperature
T_0	Reference temperature
TED	Thermoelastic damping
T_b	Cantilever thickness
T_{b_max}	Cantilever thickness at maximum Q_{total}
w	Transverse displacement
W_b	Cantilever width
x_{sv}	Molar fraction of saturated water vapor
x_v	Mole fraction of water vapor
μ	Dynamic viscosity
μ_a	Viscosity of dry air
μ_v	Viscosity of water vapor
λ	Mean free path of gas
λ_0	Reference mean free path of gas

$\overline{\lambda}$	Eigen-value
δ	Damping factor
δ_{SFD}	Damping factor of SFD
ω	Resonant frequency
ν	Poisson's ratio
α	Surface accommodation coefficient
ρ	Gas density
ρ_m	Material density

1 Introduction

Micro-cantilever, which is the most important structure of micro-electro-mechanical systems (MEMS) resonators, is successfully utilized in various MEMS sensor and transducer versatile applications such as Atomic Force Microscopes (AFM) tips and probes [1, 2] (e.g. topography, profile of surface), physical sensors (e.g. force, pressure, temperature, mass) [3, 4], chemical sensors (e.g. gases, chemical components) [5–7], bio-sensors (e.g. virus particles, bacterial, protein, molecule, DNA) [8–10], environmental monitoring (e.g. temperature, humidity) used in both gaseous and liquid states [11, 12]. The major advantages of such cantilever resonators are small size, low power consumption, extremely high sensitivity and selectivity. However, for environmental monitoring applications, the dynamic performance of micro-cantilever resonators is highly depended on the effects of temperature and humidity because high viscous damping of moist air in atmospheric pressure.

In MEMS resonators, the resonant frequency and the quality factor (Q-factor) are important outcomes for dynamic characteristics of cantilever resonators. The Q-factor is physically defined as ratio of the stored energy to its energy loss per cycle of oscillation for a resonator. High Q-factor of resonator results in high frequency stability and high sensitivity of sensing systems. An advantage of MEMS cantilever resonators is that it can operate in various environments such as vacuum, gas, and liquid. In liquid environments, low Q-factor for cantilever resonators is introduced because the vibration of cantilever is strongly resisted by high fluid viscous damping [13–15]. Namely, the density and viscosity of the fluids highly influenced on the cantilever's dynamic behavior in liquid environments [16, 17]. Therefore, Q-factor of cantilever resonators, which is very low such as Q-factor ~ 1 in pure water [18] and enhances in aqueous solution [19–21], is not exceeded 35 for transverse vibration [22, 23]. In air environment, the Q-factor is enhanced in many orders of magnitude by using of cantilevers in low viscous air damping. In MEMS cantilever resonators, the external squeeze film damping (SFD), which is a dominant damping source appeared as the gas flow squeezed in small gas spacing due to the normal motion process of vibrational structure and stationary substrate [24–28]. The internal structure damping sources such as the thermoelastic damping (TED) (loss into the structure) [29–32] and the support loss (loss into the substrate) [33, 34] are the other dominant damping mechanisms of MEMS resonators. However, the effects of temperature and humidity are main problem in air environment because cantilever dynamics are strongly influenced by the SFD. Namely, dynamic viscosity (μ) [35] of moist air changes significantly as functions of temperature and relative humidity in atmospheric pressure. Therefore, the effects of temperature and relative humidity of moist air must be carefully considered as main effects on dynamic performance of MEMS cantilever resonators. In literature review, many studies [36–38] have investigated the effect of temperature on the Q-factors of MEMS resonators under the SFD problem in atmospheric pressure. The obtained results highlighted that the Q-factor is low and strongly depended on the effect of temperature in atmospheric pressure. To improve Q-factor of resonators due to the SFD, an atmospheric pressure ($p=101{,}325$ Pa) is introduced in a small gas film spacing condition. Then, the Poiseuille flow rate (Q_P) of a gas flow occurs in a small gas film spacing (h_0) between a micro-cantilever and a substrate. To model the SFD problem, the expressions of Poiseuille flow rate (Q_P) [39–43] have been derived by solving the linearized Boltzmann equation (BGK model) for analysis of MEMS devices in wide range of inverse Knudsen number ($0.01 \le D \le 100$) and accommodation coefficients, ACs ($0.1 \le \alpha_1, \alpha_2 \le 1.0$) conditions. The accommodation coefficients, ACs ($0.1 \le \alpha_1, \alpha_2 \le 1.0$), which are the average tangential momentum exchange of the collision of gas molecules and solid surfaces, vary from 0.1 to 1.0 depending on how incident molecules scatter on solid surfaces (e.g. diffuse manners ($\alpha_1, \alpha_2=0.1$) or specular manners ($\alpha_1, \alpha_2=1.0$)), different materials and surface conditions (e.g. ACs ($\alpha_1, \alpha_2=0.7$) for polished sapphire surface or ACs ($\alpha_1, \alpha_2=0.2$) for gold surface) [44, 45]. Generally, Q_P is significantly changed with temperature and ACs (α_1, α_2) in atmospheric pressure. To consider the effects of temperature and relative humidity, the dynamic viscosity (μ) and the Poiseuille flow rate (Q_P) are used to modify the modified molecular gas lubrication (MMGL) equation for solving the SFD problem as functions of temperature and relative humidity of moist air in atmospheric pressure. Therefore, the influence of temperature and relative humidity can be carefully considered to improve the Q-factor of resonators in atmospheric pressure over wide range of ACs ($0.1 \le \alpha_1, \alpha_2 \le 1.0$). Few studies [46, 47] have discussed the effects of temperature and humidity on the Q-factor of lateral rotary micro-resonators in atmospheric pressure. Recently, the influence of temperature and humidity has experimentally been found as strong effects on the Q-factor of MEMS paddle resonators with proof mass in air environment [48]. Also, the effects of temperature and humidity have simultaneously been discussed on the frequency response of double-clamped micro-beam and cantilever resonators with the proof mass in atmospheric pressure [49]. Moreover, the effects of temperature and relative humidity on the Q-factors of MEMS cantilever resonators in wide range of ACs ($0.1 \le \alpha_1, \alpha_2 \le 1.0$) have not been discussed yet in atmospheric pressure.

In the previous work, the Q-factors of MEMS resonators are obtained by solving the MMGL equation, the transverse vibration equation of micro-cantilever, and their boundary conditions simultaneously in the eigenvalue problem [50]. The Poiseuille flow rate ($Q_P(D, \alpha_1, \alpha_2)$) is used to discuss the gas rarefaction effect in wide range of D ($0.01 \le D \le 100$) and ACs ($0.1 \le \alpha_1, \alpha_2 \le 1.0$). Then, the effects of gas rarefaction [50], surface roughness [51], temperature [52], and relative humidity [53] are separately discussed on the Q-factors of MEMS resonators in gas rarefaction. Recently, the effect of enviromental conditions on the Q-factors of MEMS resonators is only discussed in gas rarefaction [54]. However, the effects of temperature and humidity are not discussed to improve the Q-factors of MEMS cantilever resonator in atmospheric pressure. Based on the previous works, the MMGL equation is modified with dynamic viscosity ($\mu(RH, T)$) [35] and Poiseuille flow rate ($Q_P(T, ACs(\alpha_1, \alpha_2))$) [41] of moist air changed as functions of temperature (T) and relative humidity (RH) for wide range of ACs ($0.1 \leq \alpha_1, \alpha_2 \leq 1.0$) in atmospheric pressure. Then, influence of temperature and relative humidity is discussed on the Q-factors of MEMS cantilever resonators for wide range of ACs (α_1, α_2), and sizes of micro-cantilever in atmospheric pressure. The research objective is to develop a model to discuss the effects of temperature (T) and relative humidity (RH) to improve the Q-factors of MEMS resonators operating for wide range of ACs ($0.1 \leq \alpha_1, \alpha_2 \leq 1.0$) in atmospheric pressure. The obtained results can be utilized to design the higher Q-factor of MEMS temperature and humidity sensors for the environment monitoring applications based on the cantilever structure operating in atmospheric pressure.

This paper is structured as follows: the introduction section explains the ideal, theoretical background, and literature review for investigating the temperature and relative humidity dependence of Q-factors of MEMS cantilever resonators for wide range of ACs ($0.1 \leq \alpha_1, \alpha_2 \leq 1.0$) in atmospheric pressure. Section 2 shows how to obtain the Q-factor of SFD problem (Q_{SFD}) by solving the MMGL equation (which is modified by dynamic viscosity, μ (RH, T) and Poiseuille flow rate, $Q_P(T$, ACs$(\alpha_1,\alpha_2))$ as functions of temperature and relative humidity in atmospheric pressure), the linear equation of motion for transverse vibration of micro-cantilever, and their appropriate boundary conditions in the eigen-value problem. The Q-factors of TED and support loss problems are accurately included to obtain total Q-factor (Q_{total}) in wide range of cantilever sizes (length, width, and thickness). Section 3 shows the results and discussion for the significant effects of temperature and relative humidity on the dynamic viscosity (μ), the Poiseuille flow rate (Q_P), and the Q-factors (Q_{SFD}, Q_{total}) of MEMS cantilever resonators over wide range of ACs (α_1,α_2) and cantilever size (length, width, and thickness) in atmospheric pressure. In Sect. 4, the conclusions give the final scientific outcomes of the research topic.

2 Governing Equation

In this section, the SFD problem of MEMS cantilever resonators is modeled with the MMGL equation (that involves the environmental effects of temperature and relative humidity on the SFD in atmospheric pressure) for pressure variation and the equation of motion of cantilever for structural displacement. Then, the Q-factor for the SFD problem of MEMS cantilever resonator is obtained in atmospheric pressure. The dynamic viscosity ($\mu(RH, T)$) and Poiseuille flow rate ($Q_P(T, ACs(\alpha_1,\alpha_2))$, which expressed as functions of temperature and relative humidity in wide range of ACs ($0.1 \leq \alpha_1, \alpha_2 \leq 1.0$), are used to modify the MMGL equation to discuss the environmental effects of temperature and relative humidity in atmospheric pressure. The internal damping (thermoelastic damping and support loss), which is dominant damping source of MEMS cantilever resonator, is taken into account to calculate the total Q-factor of MEMS cantilever resonators. Thus, the temperature and relative humidity dependence of the Q-factors of MEMS cantilever resonators is discussed in atmospheric pressure.

2.1 The MMGL Equation for the SFD Problem of MEMS Cantilever Resonators

A new modeling approach of the effects of temperature and humidity on MEMS devices is presented in small gas film spacing (h_0) and atmospheric pressure ($p = 101{,}325$ Pa). In atmospheric pressure, the transverse motion of cantilever is strongly restricted by the SFD because the gas flow is squeezed between two parallel surfaces as showed in Fig. 1. A modified molecular gas film lubrication (MMGL) equation [41, 49] is utilized to model for the SFD problem to obtain the pressure distribution of the gas flow as below

$$\frac{\partial}{\partial x}\left(\frac{\rho h^3 Q_P(T,\alpha_1,\alpha_2)}{12\mu(RH,T)}\frac{\partial p}{\partial x}\right)+\frac{\partial}{\partial y}\left(\frac{\rho h^3 Q_P(T,\alpha_1,\alpha_2)}{12\mu(RH,T)}\frac{\partial p}{\partial y}\right)=\frac{\partial}{\partial t}(\rho h) \tag{1}$$

where ρ is the air density, h is the gas film spacing, p is the pressure, RH is the relative humidity of water vapor in moist air, and T is the temperature (°C). The Poiseuille flow rate (Q_P) [41], and dynamic viscosity (μ) of moist air [35] are used to modify the MMGL equation to discuss the environmental effects of temperature and relative humidity on the Q-factor of micro-cantilever resonator in atmospheric pressure ($p = 101{,}325$ Pa).

Moist air is a mixture of dry air and water vapor. The molar fraction of water vapor [35] is defined as a ratio of water vapor moles to total number of moles of the mixture as below

$$x_v = \frac{n_v}{n_v + n_a} = \frac{p_v}{p} \tag{2}$$

where x_v is the molar fraction of water vapor in humid air, n_v and n_a are the number of moles of water vapor and dry air, respectively. p_v is the partial pressure of water vapor, p is the partial pressure of total atmospheric pressure (1 atm).

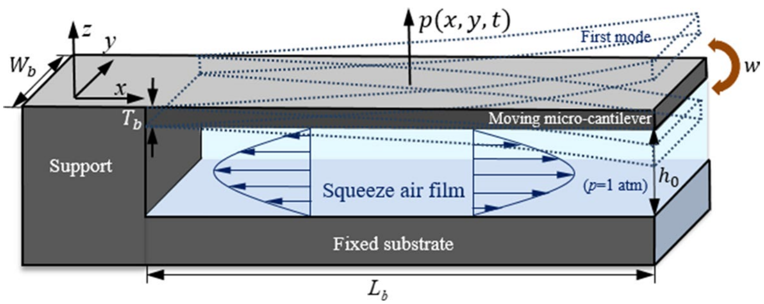

Fig. 1 Transverse vibration of micro-cantilever resonators under the SFD problem at atmospheric pressure

The relative humidity (RH) [35] is defined as the ratio of the partial pressure of water vapor in air (p_v) divided by the saturated pressure of water vapor (p_{sv}) at a given temperature as below

$$RH = \frac{x_v}{x_{sv}} = \frac{p_v}{p_{sv}} \tag{3}$$

$$\text{And } x_v = x_{sv} \cdot RH \tag{4}$$

where x_{sv} is the molar fraction of the saturated water vapor.

The molar fraction of saturated vapor pressure is corrected as function of pressure and temperature as below

$$x_{sv} = f(p, T) \cdot \frac{p_{sv}}{p} \tag{5}$$

where $f(p, T)$ is a so-called enhancement factor, which is a numerical corrective number of interaction effects between real gas molecules in air.

The molar fraction of water vapor (x_v) is then calculated from Eqs. (4) and (5) as a function of the total atmospheric pressure (p) and the saturated vapor pressure (p_{sv}) at a specific temperature as below

$$x_v = f(p, T)\frac{p_v}{p} = f(p, T) \cdot RH \cdot \frac{p_{sv}}{p} \tag{6}$$

The total atmospheric pressure (p) is given by

$$p = p_v + p_a \tag{7}$$

The correction factor, $f(p, T)$ [55] is given by

$$f(p, T) = \exp\left[\alpha \cdot \left(1 - \frac{p_{sv}}{p}\right) + \beta \cdot \left(\frac{p}{p_{sv}} - 1\right)\right] \tag{8}$$

with

$$\alpha = \sum_{i=1}^{4} A_i \cdot T^{(i-1)} \tag{9}$$

$$\beta = \exp\left(\sum_{i=1}^{4} B_i \cdot T^{(i-1)}\right) \tag{10}$$

where the numerical values of the constants in Eqs. (9) and (10) corresponding to the temperature range between 0 and 100 °C are $A_1 = 3.53624 \cdot 10^{-4}$, $A_2 = 2.93228 \cdot 10^{-5}$, $A_3 = 2.61474 \cdot 10^{-7}$, $A_4 = 8.57538 \cdot 10^{-9}$, $B_1 = -10.7588$, $B_2 = 6.32529 \cdot 10^{-2}$, $B_3 = -2.53591 \cdot 10^{-4}$, and $B_4 = 6.33784 \cdot 10^{-7}$, respectively. Therefore, typical calculated values of the enhancement factor ($f(p,T)$), which are function of temperature, are very close to unity.

The saturation water vapor pressure (p_{sv}) [49, 54] is a function of temperature (T) as below

$$p_{sv} = 1000 \cdot 0.1 \cdot 10^{e} \tag{11}$$

where

$$e = E_0 + E_1\left(1 - \frac{273}{T+273}\right) - E_2 \log_{10}\left(\frac{T+273}{273}\right) + E_3\left(1 - 10^{-8.2969\cdot\left(\frac{T+273}{273}-1\right)}\right) + E_4\left(10^{4.76955\cdot\left(1-\frac{273}{T+273}\right)}\right)$$

where E_i is interpolation constants for saturated vapor pressure such as.

$E_0 = 0.78614$, $E_1 = 10.79574$, $E_2 = 5.028$, $E_3 = 1.50475 * 10^{-4}$, and $E_4 = 0.42873 * 10^{-3}$.

The dynamic viscosity of humid air (μ) of moist air, which is calculated by the following empirical formulae [41, 53] as below

$$\mu = \frac{\mu_a \cdot (1 - x_v)}{\left[(1 - x_v) + x_v \cdot \Phi_{av}\right]} + \frac{x_v \cdot \mu_v}{\left[x_v + (1 - x_v) \cdot \Phi_{va}\right]} \tag{12}$$

where the viscosity of dry air (μ_a) and water vapor (μ_v) calculated by the following empirical formulae [35] as below

$$\mu_a = M_{A_0} + \sum_{i=1}^{4} M_{A_i}(T + 273)^i \tag{13}$$

$$\mu_v = M_{V_0} + M_{V_1}T \tag{14}$$

where MAi and MVi are interpolating constants for calculating μa and μv, respectively such as $M_{A_0} = -9.8601 \cdot 10^{-7}$, $M_{A_1} = 9.08012 \cdot 10^{-8}$, $M_{A_2} = -1.1764 \cdot 10^{-10}$, $M_{A_3} = 1.2350 \cdot 10^{-13}$, $M_{A_4} = -5.797 \cdot 10^{-17}$, $M_{V_0} = 8.058 \cdot 10^{-6}$, and $M_{V_1} = 4.0005 \cdot 10^{-8}$.

Also, Φ_{av} and Φ_{va} are interaction factors calculated as below

$$\Phi_{av} = \frac{\sqrt{2}}{4}\left(1 + \frac{M_a}{M_v}\right)^{-0.5} \cdot \left[1 + \left(\frac{\mu_a}{\mu_v}\right)^{0.5} \cdot \left(\frac{M_v}{M_a}\right)^{0.25}\right]^2 \tag{15}$$

$$\Phi_{va} = \frac{\sqrt{2}}{4}\left(1 + \frac{M_v}{M_a}\right)^{-0.5} \cdot \left[1 + \left(\frac{\mu_v}{\mu_a}\right)^{0.5} \cdot \left(\frac{M_a}{M_v}\right)^{0.25}\right]^2 \tag{16}$$

where M_a(= 28.9635) and M_v(= 18.015) are molar mass of dry air and water vapor [kg/kmol].

Under a small gas spacing, the effect of gas rarefaction becomes important to discuss in atmospheric pressure. The expression of Poiseuille flow rate

$(Q_P(D, \alpha_1, \alpha_2))$ [41] is used to modify the MMGL equation considering the gas rarefaction as follows:

$$\tilde{Q}_P(D, \alpha_1, \alpha_2) = \exp\left[\sum_{n=1}^{13} C_n (\ln D)^{13-n}\right] \tag{17}$$

$$Q_P = \frac{6}{D}\tilde{Q}_P \tag{18}$$

where $\tilde{Q}_P(D, \alpha_1, \alpha_2)$ is the Poiseuille flow rate for the gas rarefied flow.

The inverse Knudsen number (D), which is used as an important gas rarefaction indicator, is given by

$$D = \frac{\sqrt{\pi}}{2K_n} = \frac{\sqrt{\pi}h}{2\lambda} \tag{19}$$

The mean free path of gas (λ), which is estimated from kinetic theory of gases [56], can be expressed as functions of pressure (p) and temperature (T) as below

$$\lambda = \frac{RT}{\sqrt{2}\pi \cdot N_a d^2 p} \tag{20}$$

where $R = 8.314$ (J/mol) is the gas constant, $N_a = 6.0221 \times 10^{23}$ is the Avogadro's number, and d is the diameter of the cross section of gas molecular at a stable state.

At atmospheric pressure, from Eqs.(3), (7), and (20), the mean free path of moist air (λ) [52] can be expressed as functions of temperature (T), and relative humidity (RH) as follow

$$\lambda = \frac{\lambda_0 p_0 T}{p T_0} \tag{21}$$

where λ_0 is a reference mean free path of gas at a reference pressure of gas (p_0) and temperature (T_0), λ is a mean free path of gas at a pressure of gas (p) and temperature (T). Thus, the mean free path (λ) of moist air for ambient temperature (T) in atmospheric pressure ($p = 101{,}325$ Pa) can be evaluated.

2.2 The Linear Equation of Motion for Micro-Cantilever

A transverse vibration of micro-cantilever is resisted by a total pressure force ($p(x, y, t)$) of gas film per unit area of micro structure in small gap spacing as showed in Fig. 1. Under small displacement (w), the following linear form of equation of motion can be used for the transverse displacement of the micro-cantilever [57] as follow

$$D_p\left(\frac{\partial^4 w}{\partial x^4} + 2\frac{\partial^4 w}{\partial x^2 \partial y^2} + \frac{\partial^4 w}{\partial y^4}\right) + \rho_m T_b \frac{\partial^2 w}{\partial t^2} = -p(x, y, t) \tag{22}$$

where $D_p(=ET_b^3/12(1-\nu^2))$ is the cantilever flexural rigidity, E is the Young's modulus, ν is the Poisson's ratio, T_b is the cantilever thickness, $w(x, y, t)$ is the transverse displacement at positions along the cantilever (x, y), and time t, ρ_m is the material density of the cantilever. This equation is used to find the transverse displacement (w) of micro-cantilever.

The boundary conditions of the micro-cantilever are set with a clamped edge at one side $(x = 0)$ as follows

$$w(0, y, t) = 0 \tag{23}$$

$$\frac{\partial w(0, y, t)}{\partial x} = 0 \tag{24}$$

and free edges at other sides ($x = L_b$ and $y = 0$, $y = W_b$) as follows

$$\frac{\partial^2 w(L_b, y, t)}{\partial x^2} = \frac{\partial^3 w(L_b, y, t)}{\partial x^3} = 0 \tag{25}$$

$$\frac{\partial^2 w(x, 0, t)}{\partial y^2} = \frac{\partial^3 w(x, 0, t)}{\partial y^3} = 0 \tag{26}$$

$$\frac{\partial^2 w(x, W_b, t)}{\partial y^2} = \frac{\partial^3 w(x, W_b, t)}{\partial y^3} = 0 \tag{27}$$

2.3 Quality Factors of MEMS Cantilever Resonators

The Q-factor of MEMS resonators is calculated by obtaining the resultant eigenvalue $(\overline{\lambda} = \delta + i\omega)$ as the calculated procedures in Sect. 2.5 of Nguyen and Li (2016) [50]. In the eigenvalue problems [50], the Q-factor of SFD (Q_{SFD}) can be evaluated as the ratio between the resonant frequency (ω_0) (imaginary part of $\overline{\lambda}(\mathrm{Im}(\overline{\lambda}))$) and the damping factor (δ) (real part of $\overline{\lambda}$ $(\mathrm{Re}(\overline{\lambda}))$) as follows

$$Q_{SFD} = \frac{\omega_0}{2\delta} = \left| \frac{\mathrm{Im}(\overline{\lambda})}{2\mathrm{Re}(\overline{\lambda})} \right| \tag{28}$$

For MEMS resonators, the total Q-factor (Q_{total})) can be evaluated by the main contributions of Q-factor components of SFD (Q_{SFD}), TED (Q_{TED}), and support loss (Q_{sup}) [36, 37]. While the other damping mechanisms (e.g., surface loss, acoustic wave length loss, and material loss, etc.) can be neglected as follows

$$\frac{1}{Q_{total}} = \frac{1}{Q_{SFD}} + \frac{1}{Q_{TED}} + \frac{1}{Q_{\sup}} \tag{29}$$

where Q_{SFD} is obtained from the complex eigenvalue $(\overline{\lambda})$ by solving the linearized equations of Eq. (1), Eq. (22) with their appropriate boundary conditions (Eqs.

(23)–(27)) in the eigenvalue problems [50] using the Finite Element Methods (FEM). Q_{TED} is calculated by the models of Zener [29, 30] (Eq. (14) in [52]), Lifshitz and Roukes [31] (LR model) (Eq. (15) in [52]), and the FEM in COMSOL Multiphysics 5.5 [58] (Sect. 2.3 in [52]) in Fig. 13 ("Appendix A"). Q_{sup} is obtained by the theoretical model of Hao et al. [33] (Eq. (18) in [52]) in Fig. 14 ("Appendix B"). A flow chart is showed in Fig. 2 to represent for the research methodology. Thus, the effects of temperature and relative humidity on the Q-factors of MEMS cantilever resonators are discussed for wide range of ACs (α_1, α_2) and cantilever sizes (length, width, and thickness) in atmospheric pressure ($p = 101{,}325$ Pa).

3 Results and Discussion

In this section, the effects of temperature (T) and relative humidity (RH) are considered on the Q-factors of MEMS cantilever resonators in atmospheric pressure ($p = 101{,}325$ Pa). The MMGL equation (Eq. (1)) for the SFD problem is modified by the dynamic viscosity ($\mu(RH, T)$ in Eqs.(12)-(16)) and the expression of $Q_P(T, \alpha_1, \alpha_2)$ (Eqs. (17) and (18)) of moist air in [41]) in wide range of ACs(α_1, α_2) to discuss the effects of temperature (T) and relative humidity (RH) on the Q-factors (Q_{SFD}) of MEMS cantilever resonators in atmospheric pressure. Also, the Q-factors of TED (Q_{TED}) and support loss (Q_{sup}) are included to calculate the total Q-factor

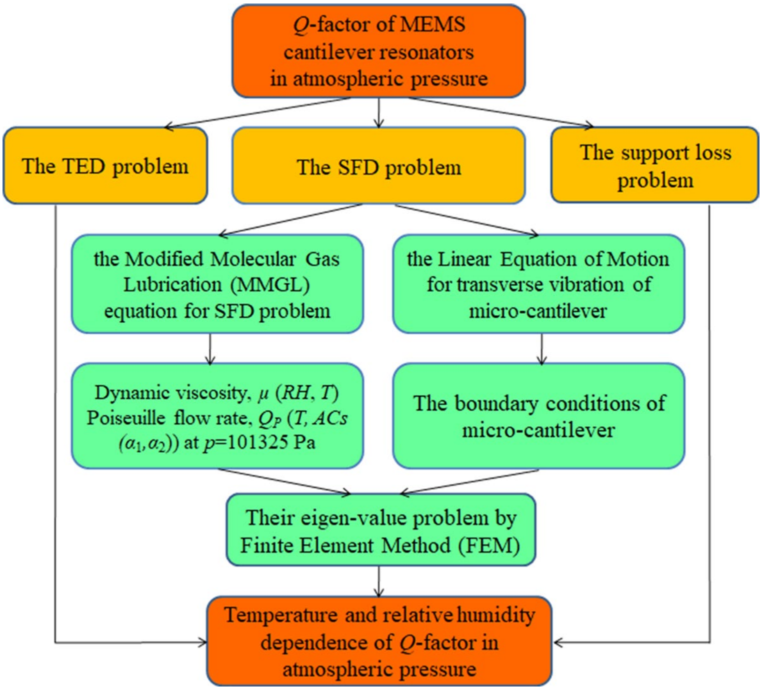

Fig. 2 Flow chart of the research methodology

(Q_{total}) of MEMS cantilever resonators in wide range of cantilever size (length, width, and thickness). Finally, the effects of temperature and relative humidity are discussed on the Q-factors (Q_{SFD}, Q_{total}) of MEMS cantilever resonators for wide range of ACs (α_1, α_2) and size of cantilever (length, width, and thickness) in atmospheric pressure.

3.1 Dynamic Viscosity, μ(RH,T) and Poiseuille Flow Rate, $Q_P(T,\alpha_1, \alpha_2)$

To discuss the effects of temperature and relative humidity on the Q-factors of MEMS cantilever resonators in atmospheric pressure, the changes in dynamic viscosity ($\mu(RH,T)$) and Poiseuille flow rate, $Q_P(T,\alpha_1, \alpha_2)$ of moist air with temperature (T) and relative humidity (RH) are simultaneously considered. In Fig. 3, the saturation water vapor pressure (p_{sv}) is plotted as function of temperature (T) by using Eq. (11). The obtained results showed that p_{sv} increases as T increases in wide range of temperature (0 °C ≤ T ≤ 100 °C) conditions. The obtained result can be used to calculate variations of dynamic viscosity (μ) of moist air as functions of temperature (T) and relative humidity (RH).

In Fig. 4, the effects of temperature and relative humidity on the dynamic viscosity of moist air are plotted by using Eqs.(12)–(16) as functions of temperature (T) and relative humidity (RH) in atmospheric pressure ($p = 101{,}325$ Pa). Dynamic viscosity (μ) of dry air constantly increases as temperature (T) increases. While, μ of moist air increases and then decreases as T increases. Also, μ decreases as relative humidity (RH) increases in wide range of temperature (T) conditions. Also, influence of relative humidity (RH) on dynamic viscosity (μ) becomes more significantly

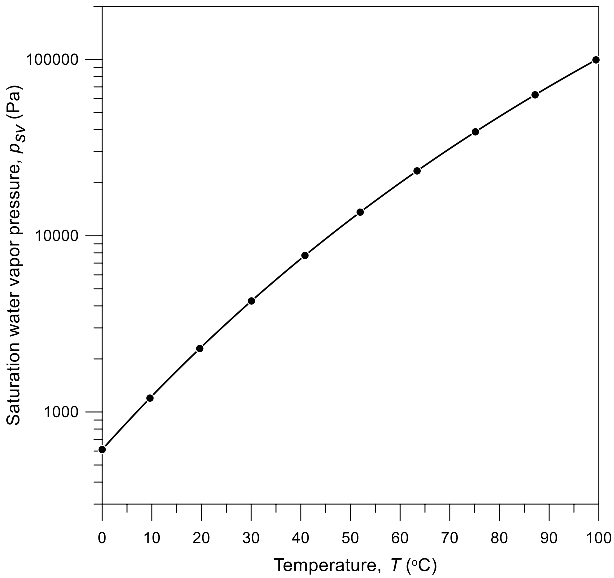

Fig. 3 Saturation water vapor pressure (p_{sv}) plotted as function of temperature (T)

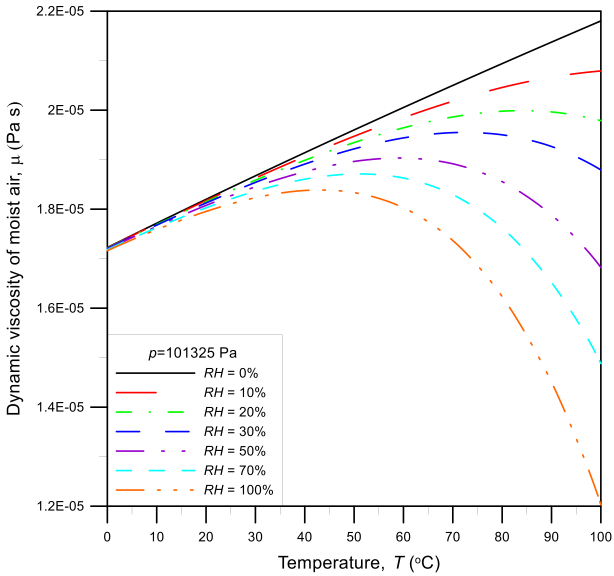

Fig. 4 Dynamic viscosity of moist air (μ) versus temperature (T) and relative humidity (RH) in atmospheric pressure ($p = 101{,}325$ Pa)

in higher T region. Thus, dynamic viscosity (μ) of moist air decreases as relative humidity (RH) and temperature (T) increase in atmospheric pressure. The obtained results can be used to discuss the effects of temperature and relative humidity on Q-factors of MEMS resonators in atmospheric pressure ($p = 101{,}325$ Pa).

In Fig. 5, the Poiseuille flow rate (Q_P) of moist air (Eqs. (17) and (18)) is plotted as function of temperature (T) for different ACs ($\alpha_1 = \alpha_2$) in atmospheric pressure ($p = 101{,}325$ Pa). The results showed that Q_P linearly increases as temperature (T) increases for different ACs ($\alpha_1 = \alpha_2$) because the mean free path of gas (λ) in Eq. (21) increases as T increases. Also, Q_P with T increases as ACs ($\alpha_1 = \alpha_2$) decrease because the gas flow becomes less restricted as ACs decrease. The obtained results of $Q_P(T, \alpha_1, \alpha_2)$ and dynamic viscosity ($\mu(RH,T)$) of moist air may be helpful to enhance the Q-factor in atmospheric pressure. Thus, the influence of temperature and relative humidity on the Q-factors (Q_{SFD}, Q_{total}) of MEMS cantilever resonators must be discussed for wide range of ACs ($\alpha_1 = \alpha_2$) and size of cantilever (length, thickness, and width) in atmospheric pressure ($p = 101{,}325$ Pa).

3.2 Effects of Temperature (T) and Relative Humidity (RH) on Resonant Frequency (ω_n), Damping Factor (δ_{SFD}), and Q-Factor (Q_{SFD})

In Fig. 6, the damping factor ($\delta_{SFD} = \mathrm{Re}\left|\bar{\lambda}\right|$) (real part of complex eigenvalue ($\bar{\lambda}$)) and Q-factor ($Q_{SFD} = \mathrm{Im}\left|\bar{\lambda}\right| / 2\mathrm{Re}\left|\bar{\lambda}\right|$) are plotted as functions of temperature (T) and relative humidity (RH) in atmospheric pressure ($p = 101{,}325$ Pa). The basic geometric and operating conditions are showed in Table 1. In Fig. 6a, the results showed

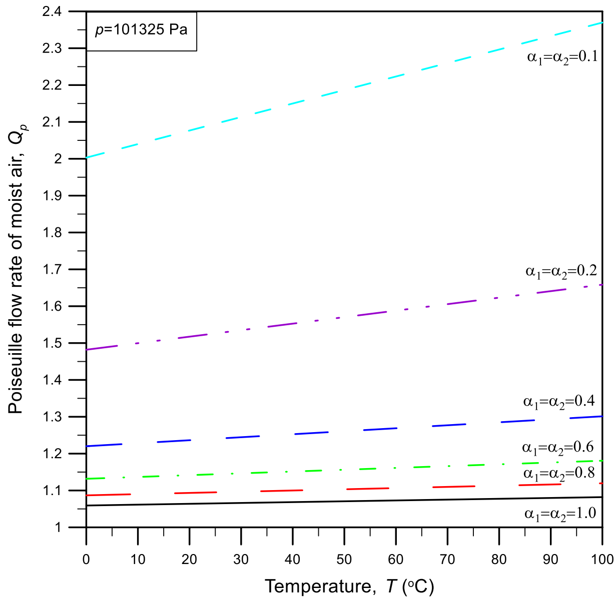

Fig. 5 Poiseuille flow rate (Q_P) of moist air versus temperature (T) for different gas rarefaction, ACs ($\alpha_1 = \alpha_2$)

that δ_{SFD} of dry air constantly increases as temperature (T) increases. While, δ_{SFD} of moist air increases and then decreases as T increases for different relative humidity (RH) conditions. Also, δ_{SFD} of moist air decreases as RH increases. δ_{SFD} of moist air decreases more considerably with RH as T increases because dynamic viscosity (μ) decreases as T and RH increase (seen in Fig. 4). This point supports that Q_{SFD} of moist air increases as relative humidity (RH) and temperature (T) increase in atmospheric pressure (as seen in Fig. 6b). Influence of relative humidity (RH) on Q_{SFD} becomes significantly as temperature (T) increases because δ_{SFD} decreases as T and RH increase and the gas flow becomes less restricted. Thus, Q_{SFD} could be enhanced as temperature (T) and relative humidity (RH) increase in atmospheric pressure.

In Fig. 7, the resonant frequency ($\omega_n = 2\pi \cdot f_n = \mathrm{Im}\left|\overline{\lambda}\right|$) (imaginary part of complex eigenvalue ($\overline{\lambda}$)), the damping factor (δ_{SFD}), and the Q-factor (Q_{SFD}) are plotted as functions of temperature (T) and relative humidity (RH) for different ACs ($\alpha_1 = \alpha_2$) in atmospheric pressure ($p=101{,}325$ Pa). In Fig. 7a, the variations of ω_n can be explained by the variations in Q_P and μ in terms of the gas film forces (the spring and damping forces discussed in Fig. 4 by [25]). The results showed that ω_n of dry air constantly decreases as temperature (T) increases. While ω_n of moist air decreases and then increases as T increases. Also, ω_n increases because μ (Fig. 4) decreases dominant (the damping and spring forces decrease) as T and RH increase in atmospheric pressure. Influence of temperature (T) and relative humidity (RH) on ω_n becomes significantly at higher ACs ($\alpha_1 = \alpha_2=1.0$), while this influence on ω_n reduces considerably at lower ACs ($\alpha_1 = \alpha_2=0.1$)) because the gas film becomes

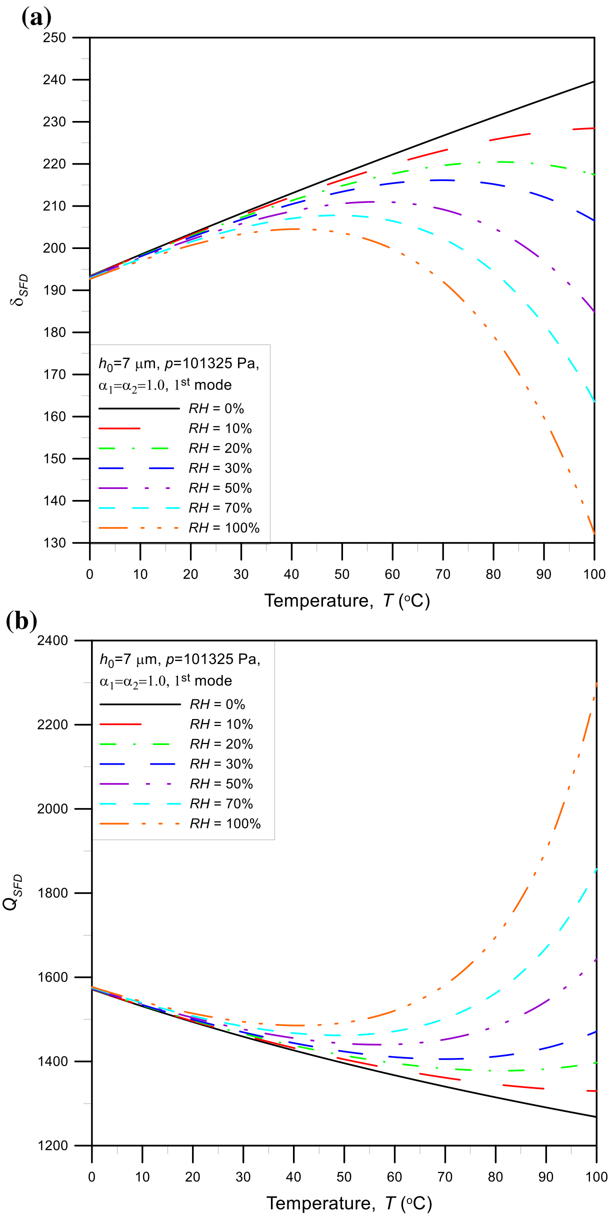

Fig. 6 **a** Damping factor (δ_{SFD}), **b** Q-factor (Q_{SFD}) versus temperature (T) and relative humidity (RH) in atmospheric pressure (p = 101,325 Pa)

less restricted and the SFD decreases as ACs ($\alpha_1 = \alpha_2$) decrease. Also, the changes of δ_{SFD} (Fig. 7b) and Q_{SFD} (Fig. 7c) with temperature (T) and relative humidity (RH) are discussed for different ACs ($\alpha_1 = \alpha_2$) conditions. The results showed that δ_{SFD} with T and RH decreases in lower ACs ($\alpha_1 = \alpha_2$) (as seen in Fig. 7b) because the

Table 1 A basic geometric and operating conditions of MEMS cantilever resonator

Symbol	Description	Values
L_b	Length of cantilever	250 µm
W_b	Width of cantilever	10 µm
T_b	Thickness of cantilever	5 µm
E	Young's modulus of silicon (100) cantilever	130×10^9 Pa
ρ_m	Density of silicon (100) cantilever	2330 kg/m^3
v	Poisson's ratio of silicon (100) cantilever	0.28
α_m	Thermal expansion coefficient of silicon cantilever	2.6×10^{-6} 1/K
κ	Thermal conductivity of silicon cantilever	90 W/(m.K)
C_P	Specific heat capacity of silicon cantilever	700 J/(kg.K)
h_0	Basic gas film thickness	7 µm
p_0	Reference ambient pressure of air	101,325 Pa
λ_{p_0}	Reference mean free path of air at pressure (p_0)	66.5 nm
T_0	Reference ambient temperature	27 °C
P	Total pressure of moist air	101,325 Pa
T	Ambient temperature	0–100 °C
RH	Relative humidity of moist air	0–100%

SFD decreases in lower ACs ($\alpha_1 = \alpha_2$). Whereas, Q_{SFD} with temperature and relative humidity increases considerably in lower ACs ($\alpha_1 = \alpha_2$) (as seen in Fig. 7c). Thus, Q_{SFD} could be increase as temperature and relative humidity increase or ACs ($\alpha_1 = \alpha_2$) decrease in atmospheric pressure.

In Fig. 8, the damping factor (δ_{SFD}), and the Q-factor (Q_{SFD}) are plotted as functions of temperature (T) and relative humidity (RH) for different length of microcantilever (L_b) in atmospheric pressure (p=101,325 Pa). The results showed that δ_{SFD} (Fig. 8a) with T and RH decreases as L_b decreases. Whereas, Q_{SFD} (Fig. 8b) with T and RH increases as L_b decreases because the δ_{SFD} decreases and the gas film becomes less restricted as L_b decreases. Furthermore, the changes of Q_{SFD} with temperature (T) and relative humidity (RH) become considerably as L_b decreases. The obtained results showed that Q_{SFD} of MEMS cantilever resonators could be enhanced with temperature and relative humidity in lower length of cantilever. Thus, the Q-factors MEMS cantilever resonators can be designed to have a strong or weak dependence on temperature and relative humidity for wide range of ACs ($\alpha_1 = \alpha_2$) and cantilever size in atmospheric pressure.

3.3 Effects of Temperature (T) and Relative Humidity (RH) on Q-Factors (Q_{SFD}, Q_{total})

The effect of cantilever size (length, width, and thickness) is a manifestation of the contributions of the SFD, TED, and support loss on the Q-factors of MEMS cantilever resonator in atmospheric pressure (p=101,325 Pa). In Fig. 9, Q-factors (Q_{SFD}) and (Q_{total}) are plotted with relative humidity (RH) and temperature (T) as function

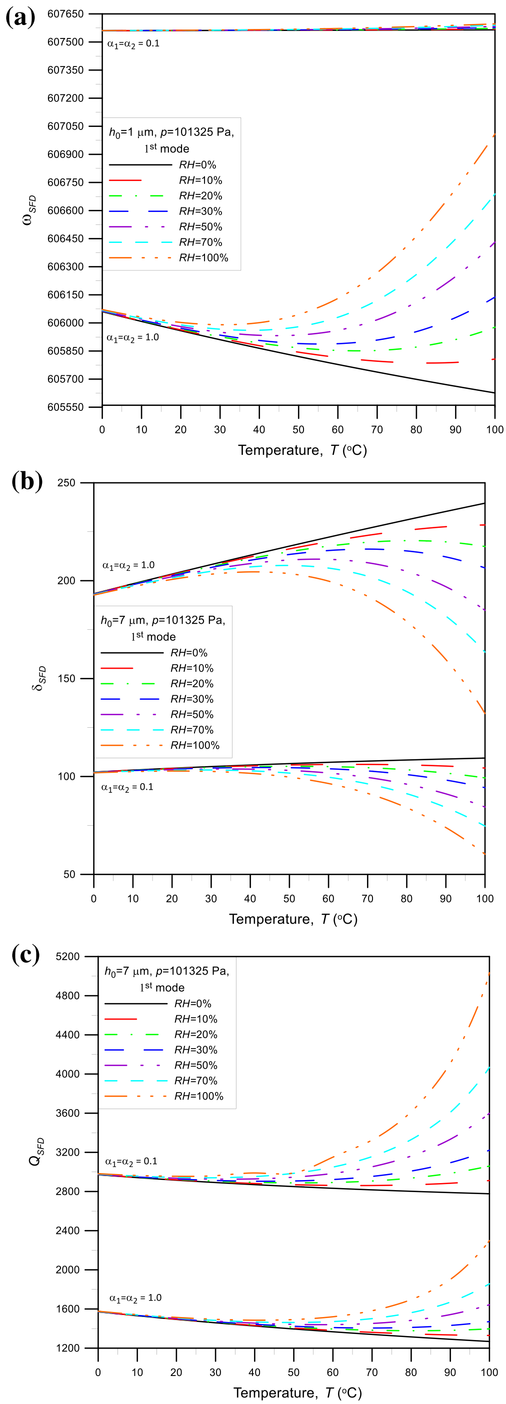

Fig. 7 **a** Resonant frequency (ω_n), **b** damping factor (δ_{SFD}), **c** Q-factor (Q_{SFD}) versus temperature (T) and relative humidity (RH) for different gas rarefaction (ACs ($\alpha_1 = \alpha_2$)) in atmospheric pressure ($p = 101{,}325$ Pa)

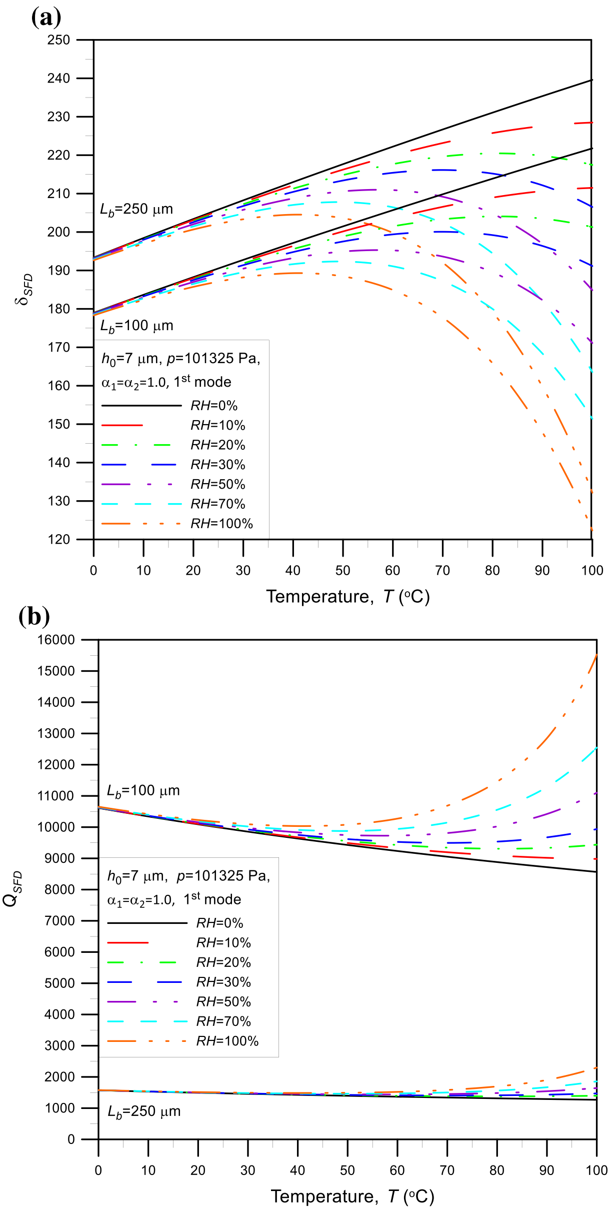

Fig. 8 **a** Damping factor (δ_{SFD}), **b** Q-factor (Q_{SFD}) versus temperature (T) and relative humidity (RH) for different length of micro-cantilever (L_b) in atmospheric pressure (p = 101,325 Pa)

of length of cantilever (L_b) for different thickness of cantilever (T_b) in atmospheric pressure. In Fig. 9a, the results showed Q_{SFD} increases as relative humidity (RH) and temperature (T) increase in wide range of length of cantilever (L_b) conditions. Also, Q_{SFD} increases considerably as relative humidity (RH) increases at higher

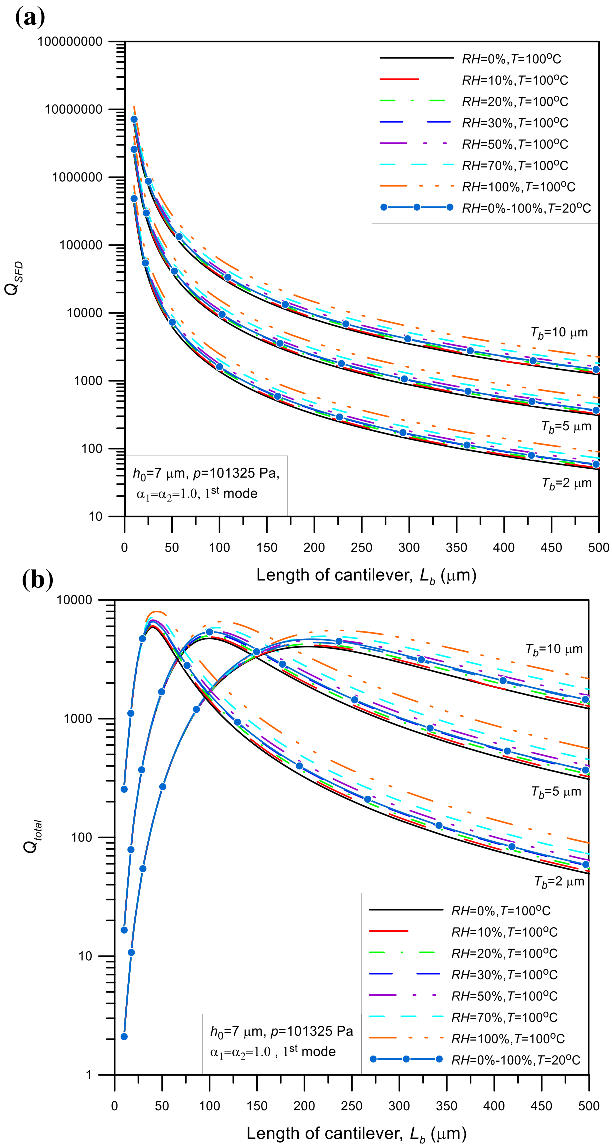

Fig. 9 **a** Q-factor (Q_{SFD}), **b** total Q-factor (Q_{total}) with temperature (T) and relative humidity (RH) versus length (L_b) for different thickness of cantilever (T_b) in atmospheric pressure ($p=101{,}325$ Pa)

temperature ($T=100$ °C). While, Q_{SFD} seems unchanged with RH at lower temperature ($T=20$ °C). The influence of RH and T on Q_{SFD} increases considerably as length of cantilever (L_b) increases because the SFD increases as L_b increases for different thickness of cantilever (T_b) conditions. In Fig. 9b, the results showed that total Q-factor (Q_{total}) with T and RH, which is calculated in Eq. (29) by the contributions of Q_{SFD}, Q_{TED}, and Q_{sup}, increases considerably up to a maximum value and then decreases as L_b increases for different T_b conditions. Q_{TED} ("Appendix A") and Q_{sup} ("Appendix B") increase significant as L_b increases because TED and support loss decrease as L_b increases. While, Q_{SFD} decreases significant as L_b increases because SFD increases as L_b increases. Also, influence of temperature and relative humidity on Q_{total} enhances considerably in greater L_b because SFD is dominant in greater L_b conditions. Whereas, temperature and relative humidity dependence of Q_{total} decreases and is neglected in lower L_b because TED and support loss become dominant in lower L_b region. Thus, maximum Q_{total} can be obtained for different relative humidity (*RH*) and temperature (*T*) in wide range of lengths of cantilever (L_b) in atmospheric pressure.

In Fig. 10, *Q*-factors (Q_{SFD}) and (Q_{total}) are plotted with temperature (*T*) and relative humidity (*RH*) as function of thickness of cantilever (T_b) for different length of cantilever (L_b) in atmospheric pressure ($p = 101{,}325$ Pa). In Fig. 10a, the results showed that Q_{SFD} increases with relative humidity (*RH*) and temperature (*T*) as thickness of cantilever (T_b) increases for different L_b conditions. In Fig. 10b, the results showed that Q_{total} with *T* and *RH* increases considerably up to a maximum value and then decreases as T_b decreases for different L_b conditions. Q_{TED} and Q_{sup} increase significantly as T_b decreases because TED and support loss decrease as T_b decreases. Whereas, Q_{SFD} decreases significantly as T_b decreases because SFD increases as T_b decreases. Influence of temperature and relative humidity on Q_{total} becomes considerably in smaller T_b because SFD is dominant in smaller T_b region. Whereas, dependence of Q_{total} on temperature and relative humidity reduces and can be neglected in greater T_b because TED and support loss become dominant in greater T_b region. Thus, maximum Q_{total} can be obtained with relative humidity (*RH*) and temperature (*T*) in wide range of thickness of cantilever (T_b) conditions in atmospheric pressure.

In Fig. 11, *Q*-factors (Q_{SFD}) and (Q_{total}) are simultaneously plotted with relative humidity (*RH*) and temperature (*T*) as functions of width of cantilever (W_b) at atmospheric pressure ($p = 101{,}325$ Pa). The results showed that Q_{SFD} increases considerably with relative humidity (*RH*) and temperature (*T*) as W_b decreases because SFD decreases as W_b decreases. The values of Q_{total} with *RH* and *T* are almost the same with those of Q_{SFD} in wide range of W_b conditions because the SFD is dominant in the 1st mode of vibration. Thus, influence of temperature and relative humidity on Q_{SFD} and Q_{total} enhances considerably as W_b increases because SFD increases and becomes dominant as W_b increases.

The obtained results showed that maximum Q_{total} can be obtained and plotted as functions of relative humidity (*RH*) and temperature (*T*) for wide range of cantilever length (L_b) and thickness (T_b) in atmospheric pressure ($p = 101{,}325$ Pa). In Fig. 12, a so-called thickness of cantilever (T_{b_max}), in which maximum Q_{total} is obtained in wide range of ACs ($\alpha_1 = \alpha_2$), is plotted as functions of relative humidity (*RH*) and temperature (*T*) for different length of cantilever (L_b). In Fig. 12a, the results showed that T_{b_max} decreases as relative humidity (*RH*) and temperature (*T*) increase in wide range of L_b conditions because Q_{SFD} increases (SFD decreases) as *RH* and *T* increase in higher ACs ($\alpha_1 = \alpha_2 = 1.0$). Also, T_{b_max} decreases with *RH* and *T* as L_b decreases because Q_{SFD} increases (SFD decreases) as L_b decreases in higher ACs ($\alpha_1 = \alpha_2 = 1.0$). Furthermore, T_{b_max} decreases

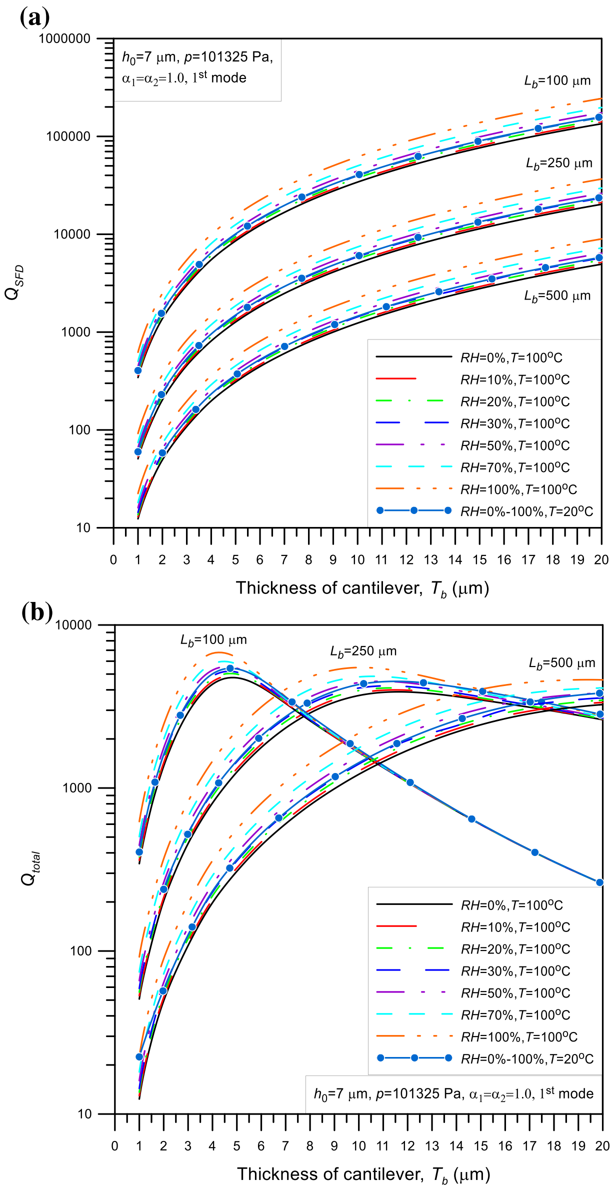

Fig. 10 **a** Q-factor (Q_{SFD}), **b** total Q-factor (Q_{total}) with relative humidity (RH) and temperature (T) versus thickness of cantilever (T_b) for different length of cantilever (L_b) in atmospheric pressure ($p = 101{,}325$ Pa)

more considerably with RH and T as L_b decreases because SFD decreases more considerably as L_b decreases in lower ACs ($\alpha_1 = \alpha_2 = 0.1$) (seen in Fig. 12b). The obtained results of T_{b_max} can be used for designer to improve the Q-factor of MEMS cantilever resonators under the effects of temperature (T) and relative

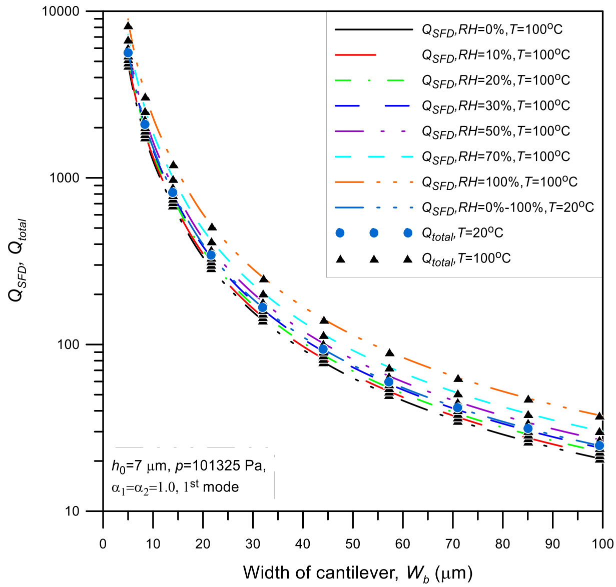

Fig. 11 *Q*-factor (Q_{SFD}) and total *Q*-factor (Q_{total}) versus width of cantilever (W_b) with relative humidity (*RH*) and temperature (*T*) in atmospheric pressure ($p = 101{,}325$ Pa)

humidity (*RH*) for wide range of ACs ($\alpha_1 = \alpha_2$) and size of cantilever in atmospheric pressure ($p = 101{,}325$ Pa).

4 Conclusions

This paper highlights the effects of temperature and relative humidity on the *Q*-factor of MEMS cantilever resonators in atmospheric pressure ($p = 101{,}325$ Pa). The SFD problem of MEMS cantilever resonator is modeled by solving the MMGL equation in wide range of temperature ($0\ ^{oC} \le T \le 100\ ^{oC}$), relative humidity ($0\% \le RH \le 100\%$), and ACs ($0.1 \le \alpha_1, \alpha_2 \le 1.0$) conditions. Dynamic viscosity ($\mu(RH, T)$) (Eqs.(12)-(16)) and Poiseuille flow rate, $Q_P(T, \alpha_1, \alpha_2)$ of moist air (Eqs.(17) and (18)) are utilized to modify the MMGL equation to consider the effects of temperature and relative humidity in atmospheric pressure ($p = 101{,}325$ Pa). The *Q*-factors of TED and support loss are also included to calculate total *Q*-factor (Q_{total}) in wide range of cantilever sizes (length, width, and thickness). Thus, the effects of temperature (*T*) and relative humidity (*RH*) on *Q*-factors (Q_{SFD} and Q_{total}) of MEMS cantilever resonators are considered for wide range of ACs ($\alpha_1 = \alpha_2$) and size of cantilever (length, width, and thickness) in atmospheric pressure ($p = 101{,}325$ Pa). Some remarkable outcomes were showed as below.

a. Q_{SFD} increases as temperature and relative humidity increase or ACs (α_1, α_2) decrease in atmospheric pressure. Influence of temperature and relative humidity on Q_{SFD} increases considerably as ACs ($\alpha_1 = \alpha_2$) decrease.

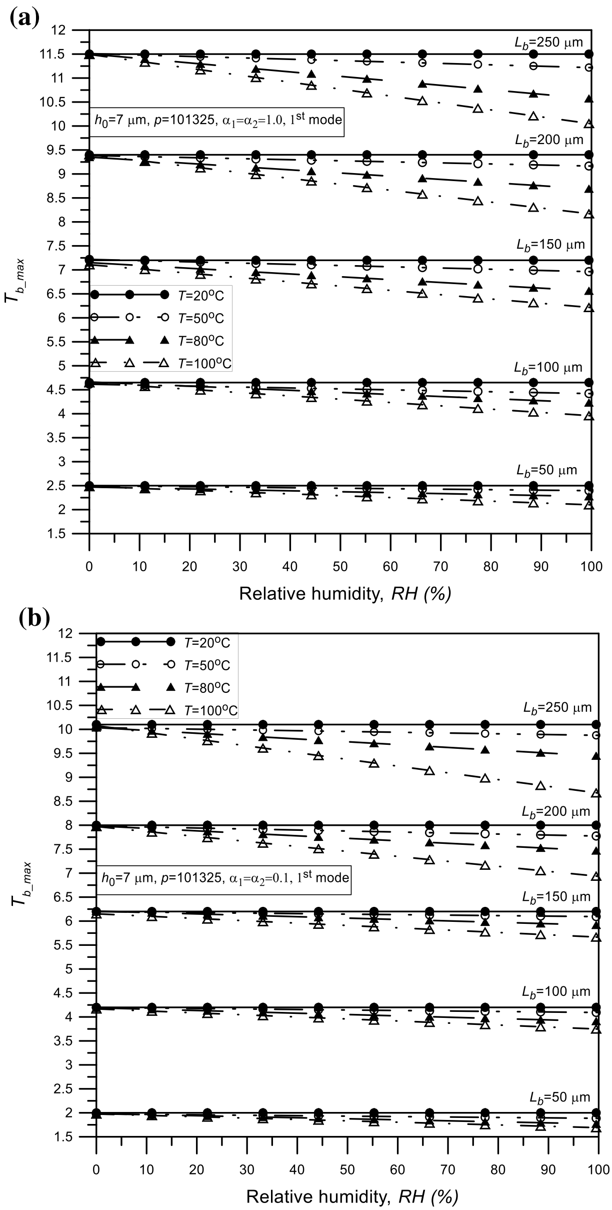

Fig. 12 Thickness of cantilever (T_{b_max}) versus temperature (T) and relative humidity (RH) for different length (L_b) of cantilever for different gas rarefaction **a** ACs ($\alpha_1 = \alpha_2 = 1.0$), **b** ACs ($\alpha_1 = \alpha_2 = 0.1$) in atmospheric pressure ($p = 101{,}325$ Pa)

b. Q_{total} with temperature and relative humidity increases up to a maximum value and then decreases as cantilever length increases and thickness decreases in atmospheric pressure. Influence of temperature and relative humidity on Q_{total}

enhances considerably because SFD is dominant in greater length and smaller thickness of cantilever. While, temperature and relative humidity dependence of Q_{total} reduces and can be neglected because TED and support loss become dominant in smaller length and greater thickness of cantilever. Finally, maximum Q_{total} of MEMS cantilever resonator can be obtained in wide range of ACs ($\alpha_1 = \alpha_2$) and cantilever size for designer to optimize the performance of MEMS temperature and humidity sensors for environmental monitoring applications in atmospheric pressure.

Appendix A

In Fig. 13, Q-factor of TED (Q_{TED}) is plotted as functions of thickness (T_b) and length of cantilever (L_b) for different temperature ($T = 20$ °C and 100 °C) in 1st mode of vibration. The present results of Q_{TED} is calculated by the modes of Zener [29, 30] (Eq. 14 in [52]) in wide range of length (L_b) and thickness (T_b) in 1st mode of cantilever. The results showed that Q_{TED} decreases to a minimum value then increases as thickness of cantilever (T_b) increases (seen in Fig. 13a). In Fig. 13b, the results showed that Q_{TED} decreases to a minimum value and then increases as length of cantilever (L_b) decreases. Minimum values of Q_{TED} are obtained because TED is very dominant at smaller L_b and greater T_b in the 1st mode of vibration. The present results of Q_{TED}, which are calculated by the models of Zener [29, 30] (Eq. (14) in [52]), can be almost the same with those obtained results of Q_{TED} by Lifshitz and Roukes [31] (LR model) (Eq. (15) in [52]), and the FEM in COMSOL Multiphysics 5.5 [58] (Sect. 2.3 in [52]) in wide range of length and thickness of cantilever. The obtained results can be used to calculate the total Q-factor (Q_{total}) in wide range of thickness and length of cantilever in atmospheric pressure ($p = 101{,}325$ Pa).

Appendix B

In Fig. 14, Q-factor of support loss (Q_{sup}) is plotted as functions of thickness (T_b) and length of cantilever (L_b) in 1st mode of vibration. The present results of Q_{sup} are calculated by the theoretical model of Hao et al. [33] (Eq. (18) in [52]). The results showed that Q_{sup} decreases as thickness of cantilever (T_b) increases (seen in Fig. 14a). Also, Q_{sup} decreases as length of cantilever (L_b) decreases (seen in Fig. 14b). Thus, Q_{sup} decreases as thickness (T_b) increases and length of cantilever (L_b) decreases because the support loss increases and becomes dominantly as T_b increases and L_b decreases in the 1st mode of vibration. The obtained results can be used to calculate the total Q-factor (Q_{total}) in wide range of thickness and length of cantilever in atmospheric pressure ($p = 101{,}325$ Pa).

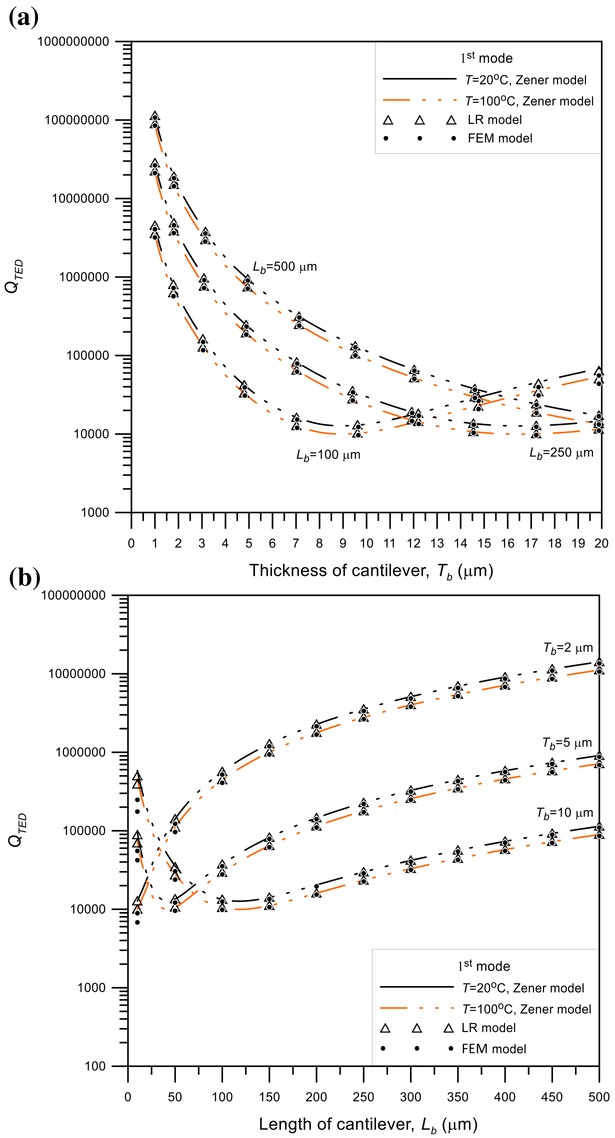

Fig. 13 Q-factor of TED (Q_{TED}) versus **a** thickness (T_b) for different length of cantilever (L_b), **b** length (L_b) for different thickness of cantilever (T_b) for different temperature (T=20 °C and 100 °C) in 1st mode of vibration

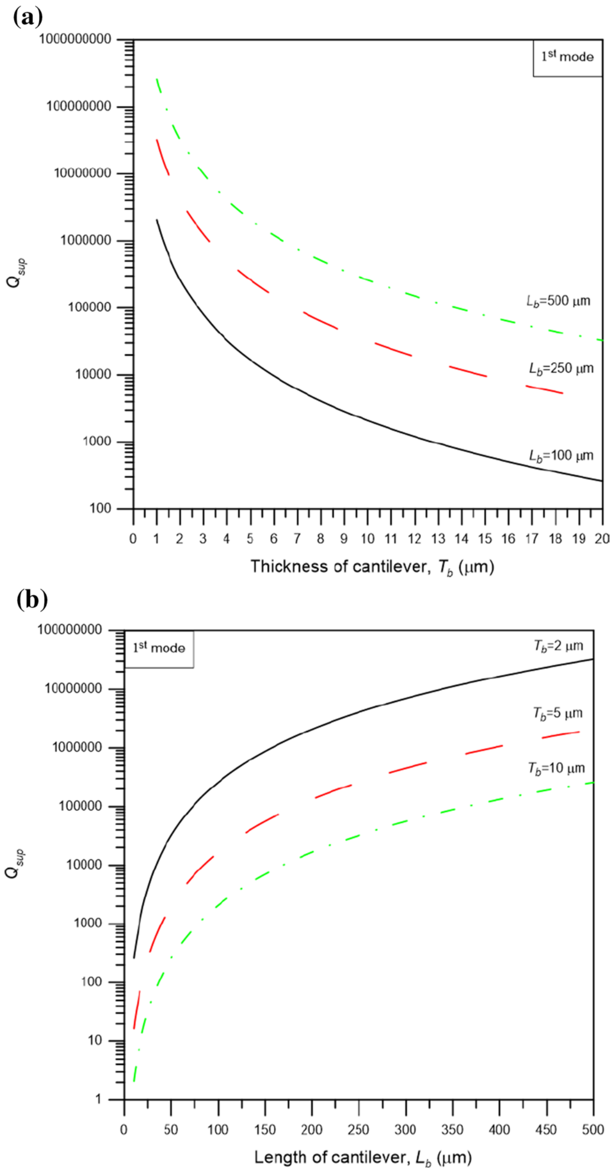

Fig. 14 *Q*-factor of support loss (Q_{sup}) versus **a** thickness (T_b) for different length of cantilever (L_b), **b** length (L_b) for different thickness of cantilever (T_b) in 1st mode of vibration

Acknowledgements This research was supported by the Institute for Computational Science and Technology (ICST), Contract Number: 08/2019/HĐ-KHCNTT in October 24th, 2019 and series number: 082019-311. Also, this research was supported by the annual projects of The Research Laboratories of Saigon High Tech Park in 2021 according to Decision No. 35/QĐ-KCNC in February 24th, 2021 and

Contract Number: 01/2021/HĐNVTX-KCNC-TTRD in March 02nd, 2021 of Management Board of Saigon High Tech Park (Project number 1).

References

1. Alunda, B. O., & Lee, Y. J. (2020). Review: Cantilever-Based Sensors for High Speed Atomic Force Microscopy. *Sensors*. https://www.mdpi.com/1424-8220/20/17/4784.
2. Kim, S., Kihm, K. D., & Thundat, T. (2010). Fluidic applications for atomic force microscopy (AFM) with microcantilever sensors. *Experiments in Fluids*. https://doi.org/10.1007/s00348-010-0830-3
3. Takahashi, H., Dung, N. M., Matsumoto, K., & Shimoyama, I. (2012). Differential pressure sensor using a piezoresistive cantilever. *Journal of Micromechanics and Microengineering*. https://doi.org/10.1088/0960-1317/22/5/055015
4. Toda, M., Inomata, N., Ono, T., & Voiculescu, I. (2017). Cantilever beam temperature sensors for biological applications. *IEEJ Transactions on Electrical and Electronic Engineering*. https://doi.org/10.1002/tee.22360
5. Baller, M. K., Lang, H. P., Fritz, J., Gerber, C., Gimzewski, J. K., Drechsler, U., Rothuizen, H., Despont, M., Vettiger, P., Battiston, F. M., & Ramseyer, J. P. (2000). A cantilever array-based artificial nose. *Ultramicroscopy*. https://doi.org/10.1016/S0304-3991(99)00123-0
6. Lang, H. P., Hegner, M., & Gerber, C. (2005). Cantilever array sensors. *Materialstoday*. https://doi.org/10.1016/S1369-7021(05)00792-3
7. Gupta, A., Akin, D., & Bashir, R. (2004). Single virus particle mass detection using microresonators with nanoscale thickness. *Applied Physics Letters. doi, 10*(1063/1), 1667011.
8. Long, Z., Kou, L., Sepaniak, M. J., & Hou, X. (2013). Recent advances in gas phase microcantileverbased sensing. *Reviews in Analytical Chemistry*. https://doi.org/10.1515/revac-2012-0034
9. Su, M., Li, S., & Dravid, V. P. (2003). Microcantilever resonance-based DNA detection with nanoparticle probes. *Applied Physics Letters. doi, 10*(1063/1), 1576915.
10. Amin, E., Habib, B. G., & Mousa, S. (2019). A novel biosensor based on micromechanical resonator array for lab-on-a-chip applications. *Sensing and Imaging*. https://doi.org/10.1007/s11220-019-0261-z
11. Nallathambi, A., & Shanmuganantham, T. (2016). Stress and sensitivity analysis of cantilever based MEMS sensor for environmental applications. *Journal of Research in Engineering and Applied Sciences.* https://doi.org/10.46565/jreas.2016.v01i01.003
12. Chen, Q., Fang, J., Ji, H. F., & Varahramyan, K. (2008). Micromachined SiO2 microcantilever for high sensitive moisture sensor. *Microsystem Technologies*. https://doi.org/10.1007/s00542-007-0489-8
13. Touaib, R., Koten, H., & Boydak, O. (2020). Parametric study of an organic rankine cycle using different fluids. *Emerging Science Journal*. https://doi.org/10.28991/esj-2020-01216
14. Kostikov, Y. A., & Romanenkov, A. M. (2020). Approximation of the multidimensional optimal control problem for the heat equation (applicable to computational fluid dynamics (CFD)). *Civil Engineering Journal*. https://doi.org/10.28991/cej-2020-03091506
15. Waghmare, M. V., Madhekar, S. N., & Matsagar, V. A. (2020). Influence of nonlinear fluid viscous dampers on seismic response of RC elevated storage tanks. *Civil Engineering Journal, 6*, 98–118.
16. Kim, D., Hong, S., Jang, J., & Park, J. (2017). Determination of fluid density and viscosity by analyzing flexural wave propagations on the vibrating micro-cantilever. *Sensors*. https://doi.org/10.3390/s17112466
17. Riesch, C., Reichel, E. K., Keplinger, F., & Jakoby, B. (2008). Characterizing vibrating cantilevers for liquid viscosity and density sensing. *Journal of Sensors*. https://doi.org/10.1155/2008/697062
18. Singh, P., & Yadava, R. D. S. (2020). Stochastic resonance induced performance enhancement of MEMS cantilever biosensors. *Journal of Physics D: Applied Physics*. https://doi.org/10.1088/1361-6463/ab98c4
19. Tamayo, J., Humphris, A. D. L., Malloy, A. M., & Miles, M. J. (2001). Chemical sensors and biosensors in liquid environment based on microcantilevers with amplified quality factor. *Ultramicroscopy*. https://doi.org/10.1016/S0304-3991(00)00082-6

20. Cyril, V., Isabelle, D., Stephen, M. H., Fabien, J., & Andreas, H. (2008). Analysis of resonating microcantilevers operating in a viscous liquid environment. *Sensors and Actuators A*. https://doi.org/10.1016/j.sna.2007.07.010
21. Fischeneder, M., Kucera, M., Hofbauer, F., Pfusterschmid, G., Schneider, M., & Schmid, U. (2018). Q-factor enhancement of piezoelectric MEMS resonators in liquids with active feedback. *Sensors and Actuators B Chemical*. https://doi.org/10.1016/j.snb.2018.01.001
22. Blake, N. J., & Raj, M. (2012). Biosensing using dynamic-mode cantilever sensors: A review. *Biosensors and Bioelectronics*. https://doi.org/10.1016/j.bios.2011.10.054
23. Schneider, M., Pfusterschmied, G., Patocka, F., & Schmid, U. (2020). High performance piezoelectric AlN MEMS resonators for precise sensing in liquids. *e & i Elektrotechnik und Informationstechnik*. https://doi.org/10.1007/s00502-020-00794-w
24. Hosaka, H., Itao, K., & Kuroda, S. (1995). Damping characteristics of beam-shaped micro-oscillators. *Sensors and Actuators A: Physical*. https://doi.org/10.1016/0924-4247(95)01003-J
25. Li, W. L. (1999). Analytical modelling of ultra-thin gas squeeze film. *Nanotechnology*. https://doi.org/10.1088/0957-4484/10/4/314
26. Lee, J. W. (2011). Analysis of fuid-structure interaction for predicting resonant frequencies and quality factors of a microcantilever on a squeeze-film. *Journal of Mechanical Science and Technology*. https://doi.org/10.1007/s12206-011-0820-2
27. Bao, M., & Yang, H. (2007). Squeeze film air damping in MEMS. *Sensors and Actuators A: Physical*. https://doi.org/10.1016/j.sna.2007.01.008
28. Pandey, A. K., & Pratap, R. (2007). Effect of flexural modes on squeeze film damping in MEMS cantilever resonators. *Journal of Micromechanics and Microengineering*. https://doi.org/10.1088/0960-1317/17/12/013
29. Zener, C. (1937). Internal friction in solids I. Theory of internal friction in reeds. *Physical Review*. https://doi.org/10.1103/PhysRev.52.230
30. Zener, C. (1938). Internal friction in solids II. General theory of thermoelastic internal friction. *Physical Review*. https://doi.org/10.1103/PhysRev.53.90
31. Lifshitz, R., & Roukes, M. L. (2000). Thermoelastic damping in micro- and nanomechanical systems. *Physical Review B*. https://doi.org/10.1103/PhysRevB.61.5600
32. Zhou, H., Li, P., & Zuo, W. (2016). Thermoelastic damping in microwedged cantilever resonator with rectangular cross-section. *in: IEEE 2016 int. conf. on mechatronics and automation (ICMA)*. https://doi.org/10.1109/ICMA.2016.7558801.
33. Hao, Z., Erbil, A., & Ayazi, F. (2003). An analytical model for support loss in micromachined beam resonators with in-plane flexural vibrations. *Sensors and Actuators A: Physical*. https://doi.org/10.1016/j.sna.2003.09.037
34. Jandak, M., Neuzil, T., Schneider, M., & Schmid, U. (2016). Investigation on different damping mechanisms on the Q factor of MEMS resonators. *Procedia Engineering*. https://doi.org/10.1016/j.proeng.2016.11.308
35. Tsilingiris, P. T. (2008). Thermophysical and transport properties of humid air at temperature range between 0 and 100 C. *Energy Conversion and Management*. https://doi.org/10.1016/j.enconman.2007.09.015
36. Nieva, P. M., McGruer, N. E., & Adams, G. G. (2006). Design and characterization of a micromachined Fabry-Perot vibration sensor for high-temperature applications. *Journal of Micromechanics and Microengineering*. https://doi.org/10.1088/0960-1317/16/12/015
37. Kim, B., Hopcroft, M. A., Candler, R. N., Jha, C. M., Agarwal, M., Melamud, , et al. (2008). Temperature dependence of quality factor in MEMS resonators. *Journal of Microelectromechanical Systems*. https://doi.org/10.1109/JMEMS.2008.924253
38. Ghaffari, S., Ng, E. J., Ahn, C. H., Yang, Y., Wang, S., Hong, V. A., & Kenny, T. W. (2014). Accurate modeling of quality factor behavior of complex silicon MEMS resonators. *Journal of Microelectromechanical Systems*. https://doi.org/10.1109/JMEMS.2014.2374451
39. Hwang, C. C., Fung, R. F., Yang, R. F., Weng, C. I., & Li, W. L. (1996). A new modified Reynolds equation for ultrathin film gas lubrication. *IEEE Transactions on Magnetics*. https://doi.org/10.1109/20.486518
40. Li, W. L. (2002). A database for couette flow rate considering the effects of non-symmetric molecular interactions. *Journal of Tribology. doi, 10*(1115/1), 1479700.
41. Li, W. L. (2003). A database for interpolation of Poiseuille flow rate for arbitrary Knudsen number lubrication problems. *Journal of the Chinese Institute of Engineers*. https://doi.org/10.1080/02533839.2003.9670799

42. Li, W. L. (2004). Modeling of head/disk interface—an average flow model. *Tribology Letters*. https://doi.org/10.1023/B:TRIL.0000044518.79255.03
43. Li, W. L. (2008). Squeeze film effects on dynamic performance of MEMS μ-mirrors-consideration of gas rarefaction and surface roughness. *Microsystem Technologies*. https://doi.org/10.1007/s00542-007-0479-x
44. Porodnov, B. T., Suetin, P. E., Borisov, S. F., & Akinshin, V. D. (1974). Experimental investigation of rarefied gas flow in different channels. *Journal of Fluid Mechanics*. https://doi.org/10.1017/S0022112074002485
45. Arkilic, E. B. (2017). Measurement of the mass flow and tangential momentum accommodation coeffcient in silicon micromachined channels, Dissertation, M.I.T, Cambridge, UK.
46. Hosseinian, E., Theillet, P. O., & Pierron, O. N. (2013). Temperature and humidity effects on the quality factor of a silicon lateral rotary micro-resonator in atmospheric air. *Sensors and Actuators A: Physical*. https://doi.org/10.1016/j.sna.2012.09.020
47. Hosseinzadegan, H., Pierron, O. N., & Hosseinian, E. (2014). Accurate modeling of air shear damping of a silicon lateral rotary micro-resonator for MEMS environmental monitoring applications. *Sensors and Actuators A: Physical*. https://doi.org/10.1016/j.sna.2014.06.008
48. Jan, M. T., Ahmad, F., Hamid, N. H. B., Khir, M. H. B. M., Shoaib, M., & Ashraf, K. (2016). Experimental investigation of temperature and relative humidity effects on resonance frequency and quality factor of CMOS-MEMS paddle resonator. *Microelectronics Reliability*. https://doi.org/10.1016/j.microrel.2016.05.007
49. Hasan, M. H. (2018). Influence of environmental conditions on the response of MEMS resonators, *Dissertation*, University of Nebraska-Lincoln.
50. Nguyen, C. C., & Li, W. L. (2016). Effect of gas rarefaction on the quality factors of micro-beam resonators. *Microsystem Technologies*. https://doi.org/10.1007/s00542-016-3068-z
51. Nguyen, C. C., & Li, W. L. (2016). Effects of surface roughness and gas rarefaction on the quality factor of micro-beam resonators. *Microsystem Technologies*. https://doi.org/10.1007/s00542-016-3140-8
52. Nguyen, C. C., & Li, W. L. (2017). Influences of temperature on the quality factors of micro-beam resonators in gas rarefaction. *Sensors and Actuators A: Physical*. https://doi.org/10.1016/j.sna.2017.04.050
53. Nguyen, C. C., Ngo, V. K. T., Le, H. Q., & Li, W. L. (2018). Influences of relative humidity on the quality factors of MEMS cantilever resonators in gas rarefaction. *Microsystem Technologies*. https://doi.org/10.1007/s00542-018-4239-x
54. Phan, M. T., Trinh, X. T., Le, Q. C., Ngo, V. K. T., & Nguyen, C. C. (2020). Effect of Environmental Conditions on Quality Factors of MEMS Cantilever Beam Resonator in Gas Rarefaction. *Sensing and Imaging*. https://doi.org/10.1007/s11220-020-00329-9
55. Greenspan, L. (1976). Functional equations for the enhancement factors for CO2-free moist air. *Journal of Research of the National Bureou of Stondards – A. Physics and Chemistry*. https://doi.org/10.6028/jres.080A.007
56. Tan, Z. (2014). *Air pollution and greenhouse gases From Basic Concepts to Engineering Applications for Air Emission Control. Green Energy and Technology*. Springer.
57. Leissa, A. W. (1969). Vibration of Plates, In: *NASA*, (pp. 1–6), Washington DC.
58. COMSOL Multiphysics 5.5. (2021). Thermoelastic Damping in a MEMS Resonator, https://www.comsol.com/model/thermoelastic-damping-in-a-mems-resonator-1439. License Date to February 1, 2021.

Authors and Affiliations

Quoc Cuong Le[1] · Minh Truong Phan[2] · Xuan Thang Trinh[3] · Huu Ly Truong[3] · Vo Ke Thanh Ngo[3] · Chi Cuong Nguyen[2,3]

1 Department of Information and Communications, 59 Ly Tu Trong street, Ben Nghe ward, district 1, Ho Chi Minh city, Vietnam

2 Institute for Computational Science and Technology, Room 311(A&B), SBI building, Quang Trung Software City, Tan Chanh Hiep ward, district 12, Ho Chi Minh city, Vietnam

3 The Research Laboratories of Saigon High-Tech-Park, Lot I3, N2 street, Saigon Hi-Tech-Park, district 9, Ho Chi Minh city, Vietnam